Available online at www.sciencedirect.com
SCIENCE DIRECT
Catalysis Today 114 (2006) 154–161
CATALYSIS TODAY
www.elsevier.com/locate/cattod

EPR and DFT study of NO interaction with Ni/SiO_2 catalyst: Insight into mechanistic steps of disproportionation process promoted by tripodal surface nickel complex

Zbigniew Sojka [a,b,c,*], Piotr Pietrzyk [a], Gianmario Martra [c,d], Maggy Kermarec [c], Michel Che [c,e]

[a] *Faculty of Chemistry, Jagiellonian University, ul. Ingardena 3, 30-060 Cracow, Poland*
[b] *Regional Laboratory of Physicochemical Analyses and Structural Research, Jagiellonian University, Ingardena 3, 30-060 Cracow, Poland*
[c] *Laboratoire de Réactivité de Surface, URA 1106, CNRS, Université P. et M. Curie, 4, Place Jussieu, 75252 Paris Cedex 05, France*
[d] *Dipartimento de Chimica Inorganica, Chimica Fisica e Chimica dei Materiali, Universita di Torino, Via P. Giuria, 10125 Turin, Italy*
[e] *Institut Universitaire de France, France*

Available online 21 February 2006

Abstract

The adsorption of NO onto Ni/SiO_2 catalyst has been investigated at 77 and 296 K at various pressures by EPR spectroscopy. The principal steps of NO disproportionation involve coordination of NO molecule with concomitant formation of paramagnetic mono $\{Ni^{II}_{3c}–NO^{\bullet}\}^9/SiO_2$ and diamagnetic dinitrosyl species $\{Ni_{2c}–(NO)_2\}^{10}/SiO_2$, reduction of nickel through inner-sphere ligand-to-metal electron transfer leading to $\{Ni^{I}_{3c}–NO^{+}\}^9/SiO_2$, formation of $\{Ni_{3c}–NO_2\}^9/SiO_2$ complex via metal-oxo intermediate, and spillover of the NO_2 ligand onto silica. The key reaction intermediates have been isolated and identified. Their assignment and molecular structure have been ascertained by DFT calculations.

Keywords: EPR; DFT; NO; NO_2; Nickel; SiO_2; Adsorption; Catalysis; Electron transfer; Disproportionation; Oxide; $deNO_x$

1. Introduction

Binding and activation of small molecules like CO, NO, O_2 diatomics or O_3, CO_2, N_2O, NO_2 triatomics by supported transition-metal ions (TMI) have been much studied for these molecules as being involved in many catalytic processes important for abatement of air pollutants [1–3]. They exhibit a versatile coordination chemistry and redox reactivity that are controlled to a large extent by a particular mode of bonding.

Although nitric oxide is thermodynamically unstable toward decomposition ($2NO \rightarrow N_2 + O_2$, $\Delta_r G^\circ = -41.3$ kcal/mol) and various disproportionation processes ($4NO \rightarrow NO_2 + N_2$, $\Delta_r G^\circ = -57.8$ kcal/mol, $4NO \rightarrow O_2 + 2N_2O$, $\Delta_r G^\circ = -32.7$ kcal/mol, $3NO \rightarrow NO_2 + N_2O$, $\Delta_r G^\circ = -24.6$ kcal/mol) [4], none of those reactions can occur to any appreciable extent without a catalyst due to the quite large kinetic stability of NO.

Owing to its particular electronic configuration with an odd electron in the π^* antibonding orbital, the chemical reactivity of a coordinated NO is featured by simple redox processes of removal of the odd electron from the π^* MO, generating the nitrosonium cation NO^+, or addition of an electron to this orbital, producing a nitroside anion NO^-. Generally, nitrosonium exhibits a tendency to a nucleophilic attack at the N-atom, while nitroside undergoes an electrophilic attack [5]. In this context, the interaction of NO with TMI, owing to various coordination modes, has received considerable interest as it can provide hints for better understanding the molecular pathways leading to elemental nitrogen.

The interaction of CO with tripodal nickel ions (Ni^{II}_{3c}) grafted to SiO_2 has been examined earlier [6,7]. Such centers can be selectively formed via molecular grafting using an appropriate precursor followed by activation at 973 K. Formation of one type of mono and two types of dicarbonyl complexes has been revealed and their detailed structure and adsorption energetics evaluated.

The present study extends previous work on the interaction of surface Ni^{II} ions with NO using EPR and IR techniques

* Corresponding author. Tel.: +48 12 663 22 95; fax: +48 12 634 05 15.
E-mail addresses: sojka@chemia.uj.edu.pl (Z. Sojka), che@ccr.jussieu.fr (M. Che).

0920-5861/$ – see front matter © 2006 Elsevier B.V. All rights reserved.
doi:10.1016/j.cattod.2006.01.016

supported by DFT calculations. Such a reaction has been investigated earlier on Ni exchanged into Y [8] and A [9] zeolites, ferrierite and mordenite [10], SAPO-34 molecular sieve [11] or synthetic clinoptilolite [12], and also on silica supported systems [2]. This paper focuses on the mechanism of NO disproportionation promoted by nickel surface complex with particular attention devoted to paramagnetic species.

2. Experimental

Ni/SiO_2 samples of 2 wt.% of nickel were prepared in aqueous ammonia via competitive ion exchange, by contacting 0.1 M $Ni(NO_3)_2{\cdot}6H_2O$ and 0.8 M NH_4NO_3 with aerosil A380 silica (Degussa, Germany, S_{BET} = 380 $m^2\ g^{-1}$). The suspension was stirred for 24 h and the pH was adjusted to 9.8 by adding ammonia. The solid was then filtered, washed with distilled water, and dried in air at 353 K for 24 h. The samples were next calcined, initially at 773 K under 160 Torr of oxygen for 15 h and then under vacuum at 973 K for 15 h. After such activation neither Ni^0 nor Ni^I species were detected by EPR.

Adsorption of NO was performed at liquid nitrogen or room temperature. Except for variable pressure experiment NO was typically adsorbed under 1–2 Torr. Prior to adsorption NO was purified by freeze-pump-thaw cycles. EPR spectra were recorded at microwave power of 2 mW at 77 K (in some cases also at room temperature) with Bruker ESR 300 and ELEXYS 500 spectrometers, both working at X-band and with 100 kHz field modulation. Spectra processing was performed with the Bruker software, while for simulation the EPRsim32 program was used [13]. In the text parameters derived from the spectra are used as convenient labels and are provided with 3-digit precision, while those obtained from simulation, which were subject to further interpretation, are given with 4-digit precision.

IR spectra were recorded after accumulation of 128 scans using a Bruker IFS 66 V spectrometer with a 4 cm^{-1} resolution. Samples in the form of self-supported wafers (ca. 20 mg in weight and 18 mm in diameter) were placed in a quartz sample holder with KBr windows.

Calculations were performed within the Kohn-Sham formalism implemented in DMol package [14]. The local spin density approximation (LSDA) with Vosko et al. [15] spin interpolation formula for correlation was used. More accurate energies were obtained by a posteriori generalized gradient (GGA) corrections to the total energy $\Delta E_{total} = E_{XC}^{GGA}[\rho^{LSDA}] - E_{XC}^{LSDA}[\rho^{LSDA}]$. The Becke [16] expression for exchange and that of Perdew and Wang [17] for correlation, denoted as BPW91, were used. As the basis set, we employed double numerical functions supplemented by polarization ones (DNP). In all cases, inner core electrons were frozen and calculations were carried out at the spin-unrestricted level.

The structures of cluster models were optimized using analytic gradients and the BFGS method, within the SCF electron density convergence criterion of 10^{-6} a.u. The optimization was based on gradient and displacement norms and energy values for which thresholds of 10^{-3}, 10^{-3} and 10^{-5} a.u. were used, respectively. The vibrational analysis was performed using harmonic approximation. The Hessian matrices were evaluated by numerical differentiation (one-point finite difference) of the analytic energy gradients using a displacement of 0.01 Bohr from the optimized geometry for all $3N$ coordinates. Magnetic parameters were calculated for previously optimized structures. Calculations of the hyperfine coupling constants were performed with the Gaussian98 program [18] using B3LYP hybrid functional together with 6–311G(d), EPR-III and LanL2DZ basis sets, justified elsewhere [19]. For $\boldsymbol{g}$ tensor calculations the ADF program [20,21] version 2002.03 was employed. The $\boldsymbol{g}$ tensors were obtained by the spin-restricted zeroth-order regular approximation (ZORA) approach [22]. Since for many transition-metal complexes they were shown to be essentially independent of the choice of a density functional [23], we applied the VWN LSDA method.

3. Results and discussion

3.1. Low temperature coordination of NO

After calcination under oxygen and subsequent evacuation the Ni/SiO_2 sample gave a very broad EPR signal (ΔB_{pp} = 200 mT) indicating the presence of Ni^{II}. The structure of this species was modeled by DFT using a **T**5 cluster $\{Si_5O_8H_8\}Ni^{II}$ described elsewhere in more detail [6,24]. In the triplet state Ni^{II} exhibited a trigonal coordination of local C_s symmetry, with one long (d_{Ni-O} = 1.939 Å) and two short nearly equidistant bonds (d_{Ni-O} = 1.784(2) Å) to surface oxygen atoms. The sum of the O–Ni–O angles, $\omega = 356^\circ$, indicated a slightly pyramidal structure of this surface complex. For the sake of brevity, it will be epitomized hereafter as a $Ni^{II}{}_{3c}/SiO_2$ (Fig. 1a).

Upon contact with 2 Torr of NO at 77 K, the sample gave rise to a new apparently axial EPR spectrum with $g_z^1 = 1.88$, $g_z^2 = 1.86$, and $g_{x,y} = 1.97$ (Fig. 2a), assigned to the adduct formed by coordination of NO to $Ni^{II}{}_{3c}/SiO_2$ [25]. A noteworthy feature of this signal is the distinct negative shift of g_z with respect to g_e, indicating that the odd electron is largely localized on the NO moiety. Indeed, at first approximation such a $\boldsymbol{g}$ tensor can be rationalized in terms of a perturbed $^2\prod_{1/2}$ radical with the unpaired electron confined in the π^* orbital that, after removal of degeneracy upon NO coordination to $Ni^{II}{}_{3c}$, is lower in energy. The orbital momentum about the NO internuclear axis is then partially quenched making the EPR signal easily observable. The local symmetry of the $\{Ni–NO\}^9$ moiety (in Enemark and Feltham notation) must be orthorhombic (or lower), since an axial crystal field cannot lift the degeneracy of the π^* levels. It rules out a linear geometry of coordination, indicating that the Ni–NO moiety exhibits a bent η^1 structure. Following classification proposed by Astruc [26] such a complex corresponds to a ligand-centered radical $\{Ni_{3c}–NO^\bullet\}^9/SiO_2$.

Two distinct values of g_z indicate two different Ni sites, as suggested by previous EXAFS data [7]. Evacuation of the samples at room temperature for 10 min, decreased the

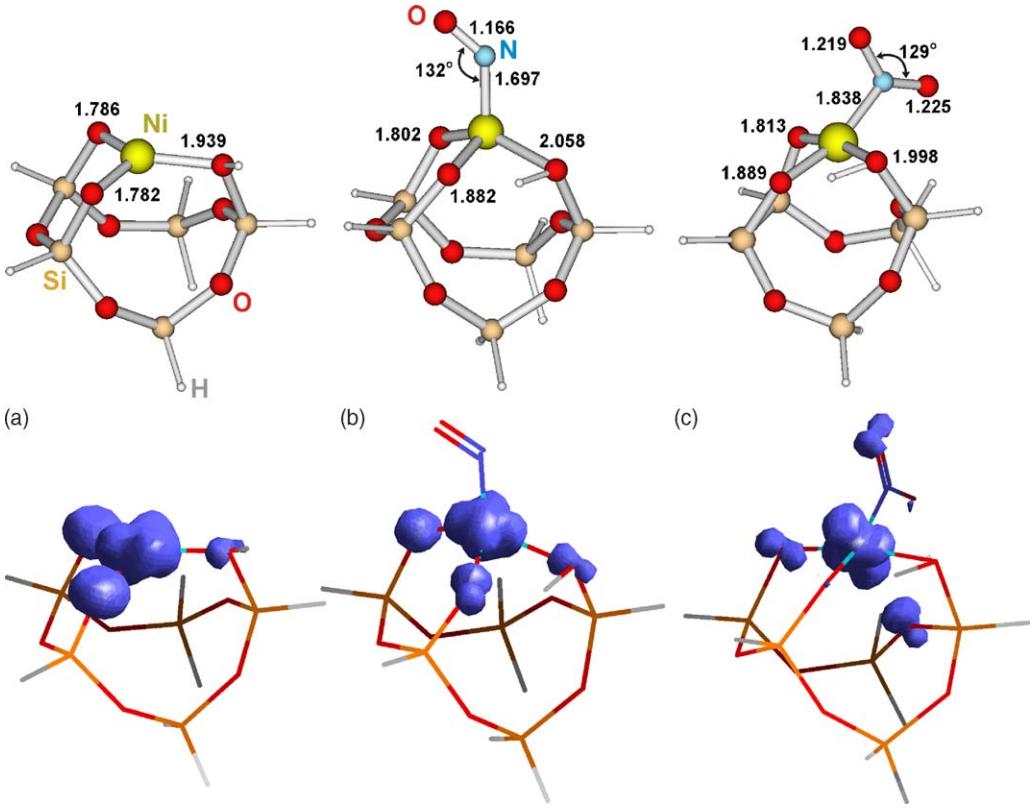

Fig. 1. Optimized VWN/DNP structures and spin density distribution of (a) Ni^{II}/SiO_2, (b) $\{Ni^{I}_{3c}–NO^{\delta+}\}^9/SiO_2$ and (c) $\{Ni_{3c}–NO_2\}^9/SiO_2$ surface complexes. All bond lengths are given in angstroms, and angles, in degrees.

intensity of the component at $g_z^1 = 1.88$ only, while the $g_z^2 = 1.86$ component completely disappeared, thus confirming the presence of two Ni sites. The initial EPR spectrum can be successfully simulated with two orthorhombic signals with $g_z^1 = 1.883$, $g_y^1 = 1.970$, $g_x^1 = 1.955$, $g_z^2 = 1.857$, $g_y^2 = 1.970$, $g_x^2 = 1.941$ (Fig. 2b). Blank experiments with adsorption of NO on bare SiO_2, pretreated exactly in the same way as the sample with nickel, gave a weak signal with g_z component at 1.98, ruling out the possibility of assignment of one of the previous species to NO trapped on the matrix.

Although the $\boldsymbol{g}$ tensor of this complex follows a general pattern $g_z < g_{x,y} \approx g_e$, its g_x component is distinctly smaller. Such a low value of g_x was observed for an intrazeolitic

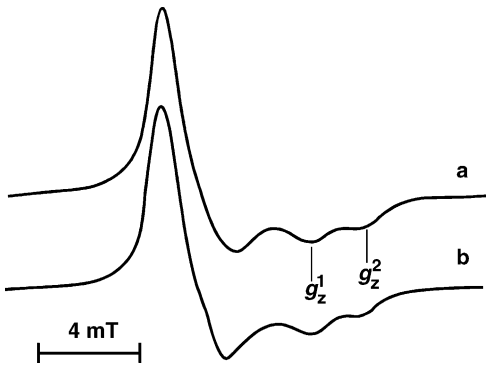

Fig. 2. (a) Experimental and (b) simulated EPR spectra (X-band, 77 K) registered after adsorption of 2 Torr of NO on Ni^{II}/SiO_2 catalyst at 77 K.

$\{NaNO\}^1$/ZSM-5 complex undergoing two-site jumping, partially averaging the g_z and g_x components [27]. The restricted mobility, as mentioned above, will also decrease the ^{14}N hyperfine structure for an odd electron in the orbital situated in the plane of motion.

Normally, for NO molecule a ^{14}N hyperfine structure is expected at least in the x direction perpendicular to the internuclear N–O axis [28]. This is in contrast to the present case, partly because the spectra are too broad in the (x,y) region (~2 mT), and also because of partial averaging of the hyperfine coupling due to restricted motion of NO in the $\{NiNO\}^9$ moiety (vide infra). The appearance of hyperfine structure may, however, also depend on the nature of the metal that NO is bonded to, and in some cases like $\{NaNO\}^1$ it was indeed not observed at 77 K by conventional EPR [27]. The upper limit for ^{14}N hyperfine splitting was therefore derived by simulating the EPR signal of the $\{Ni_{3c}–NO^{\bullet}\}^9/SiO_2$ complex by stepwise increase of the ^{14}N hyperfine constant, and comparison of the calculated and experimental spectra after adjustment of the linewidths. The limiting value $|^{N}A_x| \leq 1.7 \pm 0.2$ mT was obtained when the hyperfine features could no longer be smeared out by further line broadening. This value is in good agreement with the hyperfine splitting of 2 mT obtained for NO bonded to Ni in mordenite [10].

The EPR signal intensity of the $\{Ni_{3c}–NO^{\bullet}\}^9/SiO_2$ adduct formed at 77 K and recorded as a function of NO pressure in the range of 0.01–90 Torr (Fig. 3) exhibits a maximum at ca. 7 Torr.

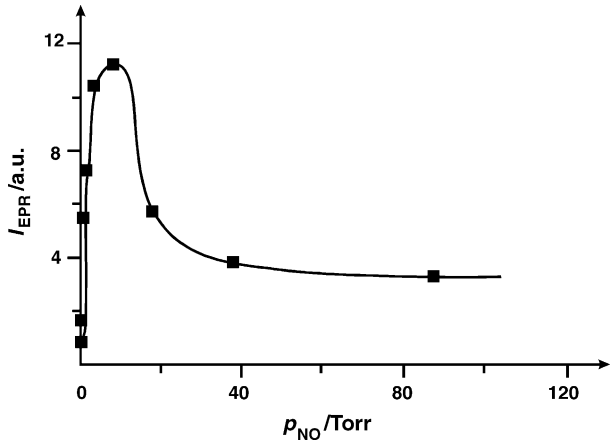

Fig. 3. EPR signal intensity of the $\{Ni_{3c}–NO^{\bullet}\}^{9}/SiO_2$ adduct as a function of NO pressure.

Except for a weak absorption at about 300 mT (corresponding to Ni^{I}) no other EPR signal was formed. It is clear that as the pressure increases, the paramagnetic mononitrosyl adduct tends to coordinate a second NO molecule to form a diamagnetic dinitrosyl $\{Ni_{2c}–(NO)_2\}^{10}/SiO_2$ surface complex, accounting for the loss of the EPR signal intensity. This process was further investigated by IR spectroscopy. The IR spectra registered after adsorption of NO ($p_{NO} \sim 0.15$ Torr) at 77 K showed two intense bands at 1882 and 1841 cm^{-1}, partially superimposed on a weaker band at 1867 cm^{-1}. Following the literature, the latter band can be assigned to the stretching frequency of nickel mononitrosyl, whereas the bands at 1882 and 1841 cm^{-1} are due to the symmetric (ν_s) and antisymmetric (ν_{as}) vibrations for the dinitrosyl complex, respectively [2,8,29].

Parallel DFT calculations revealed that binding of the first NO molecule takes place via expansion of the coordination sphere, since the number of the Ni–O(Si) bonds is preserved upon the ligation (vide infra). In contrast, coordination of the second NO molecule is an isodesmic process, as the Ni–NO bond is formed at the expense of a Ni–O(Si) bond. The resultant dinitrosyl complex, depicted in Fig. 4a, exhibited the lowest energy in a *repulso* conformation with both Ni–N–O moieties bent outwardly ($\beta = 124^{\circ}$) and with the ON–Ni–NO angle equal to $\theta = 97^{\circ}$. The calculated harmonic frequencies of such species were equal to 1860 (ν_s) and 1807 cm^{-1} (ν_{as}), in reasonable agreement with the corresponding experimental values, thus confirming the assignment.

The low temperature interaction of NO with Ni^{II}/SiO_2 can be summarized as follows:

$$\begin{aligned} &Ni^{II}{}_{3c}/SiO_2 + NO^{\bullet}{}_{(g)} \rightarrow \{Ni_{3c}–NO^{\bullet}\}^{9}/SiO_2 + NO^{\bullet}{}_{(g)} \\ &\quad \rightarrow \{Ni_{2c}–(NO)_2\}^{10}/SiO_2 \qquad (1) \\ &Ni^{II}{}_{3c}/SiO_2 + 2NO^{\bullet}{}_{(g)} \rightarrow \{Ni_{2c}–(NO)_2\}^{10}/SiO_2. \end{aligned}$$

Apparently, both mono and dinitrosyl complexes are formed simultaneously and coexist in a wide pressure range, since the EPR signal of $\{Ni_{3c}–NO^{\bullet}\}^{9}/SiO_2$ persists even at $p_{NO} > 80$ Torr, where the dinitrosyl complexes were far more dominant.

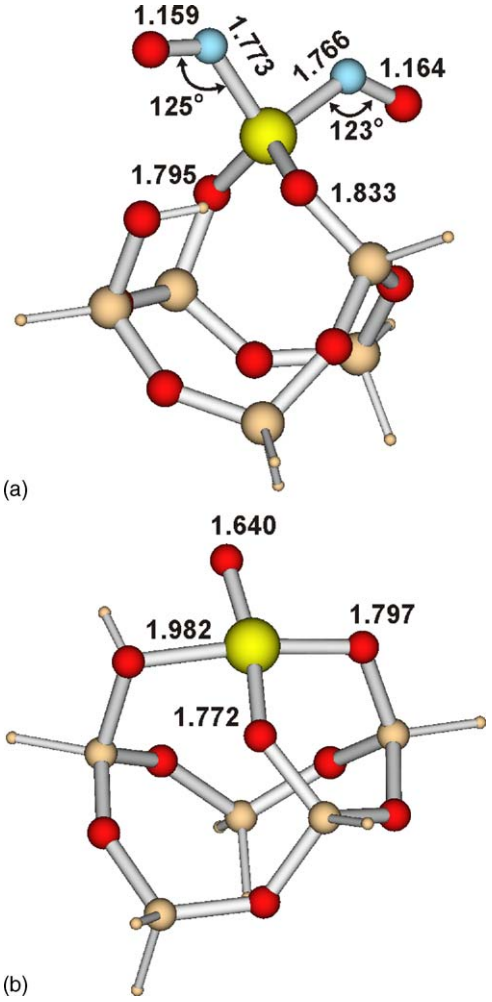

Fig. 4. Optimized VWN/DNP structures of (a) $\{Ni_{2c}–(NO)_2\}^{10}/SiO_2$ in repulso conformation, and (b) $\{^{3}Ni_{3c}{=}O\}^{8}/SiO_2$ surface complexes. All bond lengths are given in angstroms, and angles, in degrees.

In contrast to what has been observed in zeolite A [9], neither an EPR signal due to $(NO)_2$ nor appreciable dipolar broadening of the $\{Ni_{3c}–NO^{\bullet}\}^{9}/SiO_2$ spectrum were observed. This indicates that the distance between the nitrosyl complexes is greater than ca. 0.5 nm (below which the spins tend to interact), confirming a good dispersion of Ni ions.

3.2. Reductive coordination of NO

Adsorption of NO at $p_{NO} \geq 2$ Torr at 296 K with immediate cooling to 77 K, produced an axial signal with $g_{||} = 2.23$ and $g_{\perp} = 2.11$, which can be assigned to Ni^{I} ions [30,31]. Prolonged exposure (4 h) at room temperature led to distinct modification of this signal, manifested by the shift of both g values ($g_{||} = 2.36$ and $g_{\perp} = 2.15$). The appearance of the Ni^{I} signal indicates that divalent nickel is readily reduced by NO. This was further revealed by the EPR experiments (spectra recorded at 77 K) where NO was first admitted at 77 K (Fig. 5a) and next warmed to 296 K for various periods of time (Fig. 5b–d). The signal of the $\{Ni_{3c}–NO^{\bullet}\}^{9}/SiO_2$ adduct initially slightly increased (most probably due to readsorption of some NO trapped on the walls

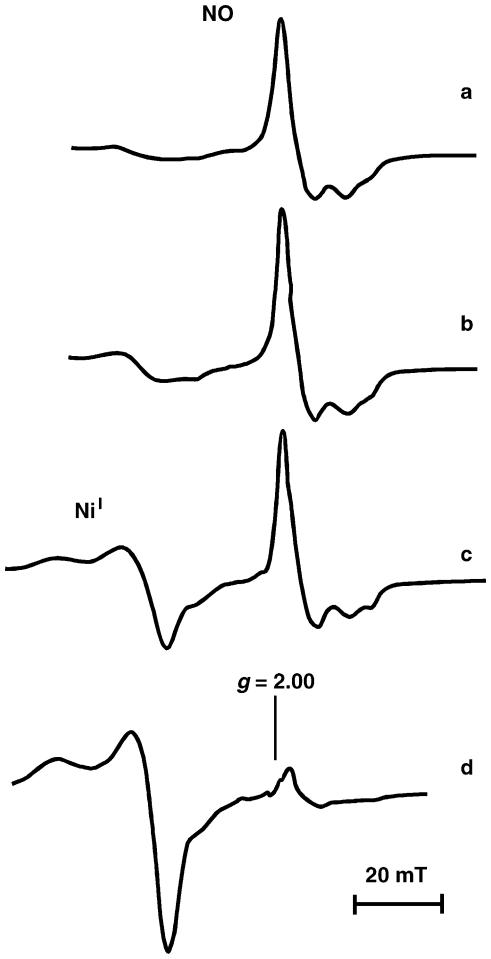

Fig. 5. EPR signal (X-band, 77 K) obtained after contact of 2 Torr of NO with Ni^{II}/SiO_2 at 77 K and after warming to 296 K for (a) 0.5 min, (b) 17 min, (c) 107 min and (d) 200 min.

of the EPR cell) and then gradually decreased (Fig. 5b–d). At the same time, a pseudoaxial signal with $g_{||} = g_z > g_\perp = 1/2(g_x + g_y) > g_e$, observed earlier after adsorption of NO at room temperature, gradually developed.

The simulation revealed that this signal can be fitted assuming an orthorhombic symmetry with $g_z = 2.369$, $g_y = 2.184$, $g_x = 2.156$. Following the literature, we assigned it to a $\{Ni^{I}{}_{3c}–NO^{\delta+}\}^9/SiO_2$ adduct [32] with the unpaired electron localized virtually on the metal side, leading to an EPR spectrum typical of Ni^{I} formed via inner-sphere ligand-to-metal electron transfer (LMET), converting the NO ligand into an electrophilic nitrosonium ($NO^{\delta+}$) species.

$$\{Ni_{3c}–NO^{\bullet}\}^9/SiO_2 \rightarrow \{Ni^{I}{}_{3c}–NO^{\delta+}\}^9/SiO_2 \quad (2)$$

The $\boldsymbol{g}$ tensor values of this complex, very close to those found earlier for distorted tetrahedral Ni^{I} ions bound to three lattice oxygens and one NO ligand [33], can be best rationalized in terms of a C_s structure close to a distorted square planar symmetry with $d_{x^2-y^2}$ ground state [34].

More insight into the molecular structure of the nickel nitrosonium adduct was obtained by DFT calculations. The geometry of this complex is shown in Fig. 1b, along with the associated spin density contour. The spin density is mainly confined to the metal center (61%) with sizeable part spread onto the matrix ligands (37%), and only 2% localized on the NO moiety, accounting well for the formulation of the $\{Ni^{I}{}_{3c}–NO^{\delta+}\}^9/SiO_2$ complex in terms of a metal-centered radical. The original tridentate coordination of the Ni ion to the framework (assignment of the Ni coordination number was based on the bond length criterion $d_{Ni–O} < 2.5$ Å), is maintained upon formation of the nitrosonium Ni^{I} complex. The latter shows a C_s local symmetry with the mirror plane bisecting the angle $\delta_{O–Ni–O}$ defined by the bonds between Ni and the two proximal oxygen atoms (Fig. 1a and b). The bound NO molecule was tilted toward the shorter Ni–O bonds, to make a Ni–N–O angle of 132°. Such a bending was previously observed and interpreted in terms of increased $3d–2\pi^*$ interaction [35]. The distance $d_{Ni–N} = 1.697$ Å was distinctly shorter than that observed in the akin $\{CuNO\}^{11}$/ZSM-5 species ($d_{Cu–N} = 1.890$ Å) [19]. Interestingly, despite the significant activation (transfer of the unpaired electron to the metal center), the N–O distance ($d_{N–O} = 1.166$ Å) remained almost unaffected.

The concomitant variation of the Ni bonding to the framework consisted mainly in an appreciable decrease of the (Si)O–Ni–O(Si) angle ($\omega = 328°$) in comparison to the parent $Ni^{II}{}_{3c}/SiO_2$ surface complex ($\omega = 357°$), while the average Ni–O(Si) distance $\langle d_{Ni–O} \rangle$ was considerably elongated from 1.836 to 1.914 Å, respectively. The calculated stretching frequency of the NO ligand, $\nu = 1845$ cm^{-1}, and the theoretical $\boldsymbol{g}$ tensor ($g_z = 2.241$, $g_y = 2.053$, $g_x = 2.046$) remain in reasonable agreement with the corresponding experimental values.

Although this type of chemistry has been already described [8–11], there has been so far no attempt to assess the energy

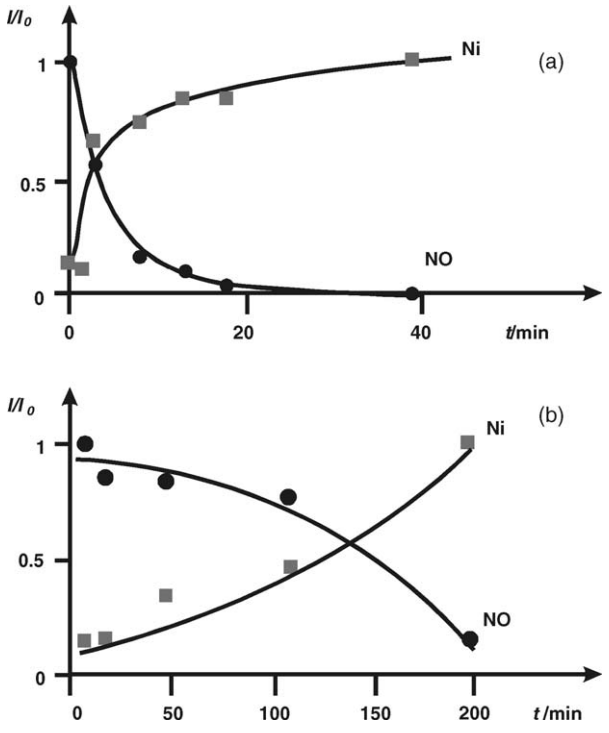

Fig. 6. Variation of the EPR signal intensity of $\{Ni_{3c}–NO^{\bullet}\}^9/SiO_2$ (●) and $\{Ni^{I}{}_{3c}–NO^{\delta+}\}^9/SiO_2$ (■) species as a function of time at (a) 373 K and (b) 296 K.

barrier of the ligand-to-metal electron transfer (LMET) process from kinetic studies. Fig. 6 shows typical plots of the intensity of the EPR signals due to $\{Ni_{3c}–NO^{\bullet}\}^9/SiO_2$ and $\{Ni^{I}_{3c}–NO^{\delta+}\}^9/SiO_2$ complexes as a function of time at 373 and 296 K. It indicates that one species is formed at the expense of the other, in accordance with the reaction stoichiometry (Eq. (2)). From the corresponding semi-logarithmic plots ($\ln I/I_0 = kt$) an apparent activation energy $E_a = RT_1T_2/(T_2 - T_1)\ \ln(k_2/k_1)$ for LMET was determined to be $E_a = 10 \pm 3$ kJ/mol, in the range of 290–400 K. This value is largely dictated by the inner-sphere reorganization energy of the Ni center (modifications of bond lengths and angles in the tripodal Ni^{II} complex upon reduction to Ni^{I}), since as unraveled by DFT calculations the N–O bond shortening on going from $NO^{\bullet}$ to $NO^{\delta+}$ was rather insignificant. The value of the activation energy may be compared to that of $E_a = 20$ kJ/mol, previously found for MLET process between N_2O and surface molybdenum in the MoO_x/SiO_2 system [36]. The latter is associated with the vibrational preactivation of the N_2O molecule (bending of the N–N–O angle), which is in this case a necessary prerequisite for making the MLET feasible.

The $\{Ni^{I}_{3c}–NO^{\delta+}\}^9/SiO_2$ adduct was partially destroyed (the initial signal intensity decreased about three times) upon evacuation at room temperature for 1.5 h, whereas outgassing at 400 K for 15 min destroyed it almost completely. However, after 5 min of contact with NO readmitted at room temperature, the original signal was restored, revealing at least partial reversibility of the metal–ligand redox process. Simultaneously, a weak signal attributable to NO_2 radical was detected at the high field part of the spectrum. Formation of this species is discussed in the next section.

3.3. Surface disproportionation of NO

The evolution of EPR spectrum of $\{Ni^{I}_{3c}–NO^{\delta+}\}^9/SiO_2$ as a function of time at room temperature is shown in Fig. 7. The initial EPR signal of Ni^{I} (at low field of the spectrum) faded away in time while a new anisotropic signal with hyperfine structure gradually appeared. The characteristic shape and the position of this signal, very similar to that found earlier by Lunsford [37] on MgO and Zomack on Xe/Ag(1 1 1) [38], provides clear evidence for its assignment to adsorbed, fairly rigid NO_2 species. The splitting into three lines ($m_I = -1, 0, +1$) can be then explained by the hyperfine interaction of the odd electron with the ^{14}N nucleus ($I = 1$, 98% natural abundance).

The magnetic parameters of the NO_2 spectrum were determined by simulation assuming an orthorhombic spin-Hamiltonian with $g_z = 2.002$, $g_y = 1.992$, $g_x = 2.004$, $|^{N}A_z|/g\beta_e = 6.32$ mT, $|^{N}A_y|/g\beta_e = 4.78$ mT and $|^{N}A_x|/g\beta_e = 5.15$ mT. The values of the $\boldsymbol{g}$ and $^{N}\boldsymbol{A}$ tensors are similar to those observed for NO_2 on various surfaces [39]. In all cases, two g_i components are around the free electron value ($g_e = 2.0023$), while one corresponding to the O–O direction is distinctly smaller (this is also the direction of the smallest hyperfine constant). This negative shift results from mixing of the ground state singly occupied molecular orbital (SOMO) with the relatively low-lying lowest unoccupied molecular orbital (LUMO), which differ in energy as a function of the NO_2 bending. The $^{N}\boldsymbol{A}$ tensor was conventionally decomposed into isotropic $a_{iso}/g\beta_e = 5.42$ mT and dipolar components $^{N}\boldsymbol{T}/g\beta_e = |0.9, -0.64, -0.27|$ mT. The resulting contributions of the nitrogen s, p_z and p_x orbitals to SOMO were found to be $c^2(2s) = 0.099$, $c^2(2p_z) = 0.30$ and $c^2(2p_x) = 0.074$. The unpaired electron is thus mainly confined to the nitrogen $2p_z$ orbital.

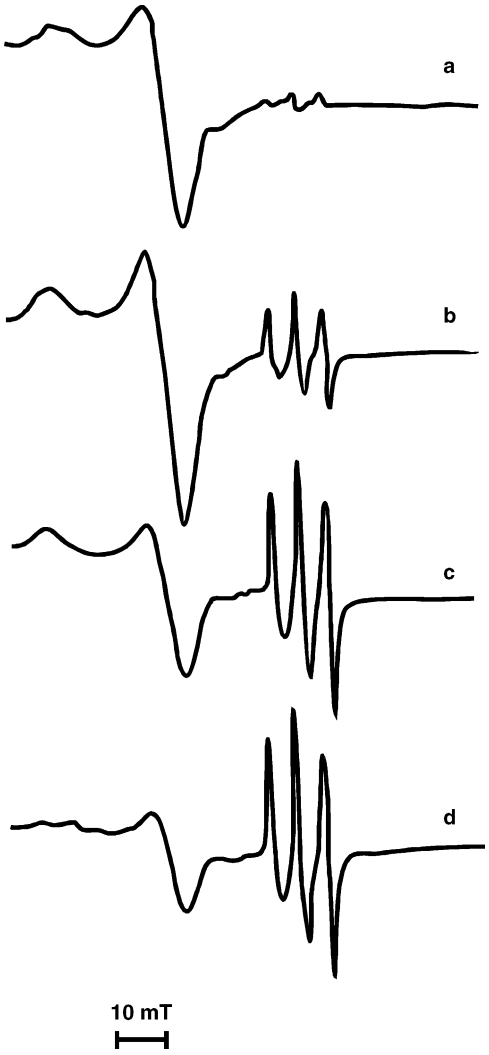

Fig. 7. EPR spectra of the Ni^{II}/SiO_2 sample after readmission of 2 Torr of NO at 77 K and warming to room temperature for (a) 5 min, (b) 0.5 day, (c) 2 days and (d) 4 days.

From comparison of the DFT calculated EPR parameters for silica-trapped NO_2 ($g_z = 2.002$, $g_y = 1.986$, $g_x = 2.007$, $a_{iso}/g\beta_e = 5.6$ mT) and for the $\{Ni_{3c}–NO_2\}^9/SiO_2$ complex ($g_z = 2.424$, $g_y = 2.114$, $g_x = 1.951$, $a_{iso}/g\beta_e = 0.149$ mT) with experiment, it can be readily concluded that the observed NO_2 radical is trapped on the SiO_2 support. Indeed, in a blank experiment, where NO_2 was adsorbed on bare silica activated in the same way as the Ni/SiO_2 catalyst, virtually the same EPR spectrum was obtained, confirming that NO_2 produced by reaction of NO with the $\{Ni^{I}_{3c}–NO^{\delta+}\}^9/SiO_2$ complex spills over to SiO_2. Spillover of radicals has also been observed in the case of MoO_x/SiO_2 catalyst and Co_xMgO_{1-x} solid solutions, where O_2^- species, initially formed via electron transfer at the

transition-metal centers, subsequently migrate to the matrix because of an important configurational entropy gain [40,41].

Analysis of the EPR results indicates that the mechanism of the reaction leading to NO_2 is quite involved and apparently depends on the pressure of NO. Furthermore, separate IR experiment showed that the appearance of NO_2 is accompanied by the formation of N_2O, which at least from a stoichiometric view point, can be accounted for by the disproportionation of NO written as follows:

$$\{Ni^{I}{}_{3c}{-}NO^{\delta+}\}^{9}/SiO_2 + 2NO_{(g)} \rightarrow \{Ni_{3c}{-}NO_2\}^{9}/SiO_2 + N_2O. \quad (3)$$

Initially only NO_2 remains coordinated as N_2O is known to be a poor ligand [42].

Such disproportionation of NO promoted by transition-metal complexes is well established and is best exemplified by Co, Ir, and Rh complexes [43]. For non-reducing ligands such as surface oxygens, N_2O is typically produced, and the reaction occurs stepwise rather than in a concerted manner. At higher pressure of NO an inner-sphere dissociative mechanism, proposed earlier for Cu supported on silica or exchanged into zeolites [44], can be reconciled with the spectroscopic and DFT data. The reaction can be initiated either by an attack of gas phase NO on the ligand (coordinated $NO^{\delta+}$) or by an attack on the metal (Ni^{I} center). The actual direction is controlled by the spin density redistribution within the $\{Ni–NO\}^9$ moiety [45]. Since the spin density is largely localized on nickel (Fig. 1b), the formation of the spin-paired dinitrosyl species $\{Ni_{2c}–(NO)_2\}^{10}/SiO_2$ is preferred as confirmed by IR spectra. Thermal decomposition leads to the formation of a nickel-oxo derivative through oxygen transfer with N_2O as a byproduct:

$$\{Ni^{I}{}_{3c}{-}NO^{\delta+}\}^{9}/SiO_2 + NO_{(g)} \rightarrow \{Ni_{2c}{-}(NO)_2\}^{10}/SiO_2 \rightarrow \{Ni_{3c}{=}O\}^{8}/SiO_2 + N_2O. \quad (4)$$

The resultant nickel-oxo moiety (Fig. 4b) corresponds to an extra-lattice oxygen (ELO), typically invoked as intermediate in deNO_x and deN_2O reactions [43,44,46]. From our DFT calculations it is shown that in the triplet state, situated 7.8 kcal/mol below the singlet, the nickel-oxo moiety exhibits a distorted square planar coordination with the average Ni–O(Si) bond length of $\langle d_{Ni–O(Si)}\rangle$ = 1.85 Å, and a shorter nickel-oxo bond ($d_{Ni–O}$ = 1.64 Å). The spin density, unevenly distributed within the $\{Ni_{3c}{=}O\}^8$ moiety (39.5% on Ni, 53.2% on O, and 7.3% on silica), is distinctly shifted towards the oxygen, which becomes a preferred site for subsequent NO attack. This suggests that the Ni-bound NO_2 evolves by subsequent reaction of a second NO molecule with $\{Ni_{3c}{=}O\}^8/SiO_2$ as follows:

$$\{Ni_{3c}O\}^{8}/SiO_2 + NO_{(g)} \rightarrow \{Ni_{3c}{-}NO_2\}^{9}/SiO_2. \quad (5)$$

From four possible coordination modes (η^1-*N*$\{Ni–NO_2\}^9$, η^1-*O*$\{NiNO_2\}$, η^2-*O*,*O*$\{Ni–NO_2\}^9$, and η^2-*N*,*O*$\{Ni–NO_2\}^9$), DFT calculations revealed that for the $\{Ni_{3c}–NO_2\}^9/SiO_2$ complex the monodentate nitrite form η^1-*N*$\{Ni–NO_2\}^9$ (Fig. 1c) is the most stable (ΔE_{ads} = −16.7 kcal/mol). The magnetic parameters calculated for such species are consistent with the spin density localized on Ni^{I} with the $d_{x^2-y^2}$ ground state of S = 1/2, making the EPR spectrum quite similar to that of the parent $\{Ni^{I}{}_{3c}–NO^{\delta+}\}^9/SiO_2$ complex with the same ground state. Thus, formally the nickel center is reduced back to Ni^{I} in this reaction step. The only appreciable difference can be seen in the structurally most sensitive g_z component, which is expected to be slightly larger. Indeed in the EPR spectrum upon prolonged contact with NO, a new low field feature in the g_z region, which can be associated with the $\{Ni_{3c}–NO_2\}^9/SiO_2$ complex, could readily be observed (Fig. 7).

Because of the apparent lability of the $\{Ni_{3c}–NO_2\}^9/SiO_2$ complexes, arising from relatively small Ni–NO_2 binding energy, the NO_2 ligands tend to leave the coordination sphere of nickel and migrate onto SiO_2. This can be easily inferred from the characteristic triplet EPR signal, appearing in the high field part of the EPR spectrum, steadily growing in the intensity (Fig. 7).

$$\{Ni_{3c}{-}NO_2\}^{9}/SiO_2 \rightarrow Ni^{II}{}_{3c}/SiO_2 + NO_2/SiO_2. \quad (6)$$

The EPR signals of both the Ni^{I}-containing complex and the NO_2 trapped on silica were partially destroyed by outgassing at 400 K for 15 min, and completely eliminated after 30 min of evacuation at 400 K. However, readsorption of nitric oxide restored the EPR spectrum of the parent $\{Ni^{I}{}_{3c}–NO^{\delta+}\}^9/SiO_2$ complex, proving not only a full reversibility of the oxidation states of nickel, but also its persistent ability for binding NO, which is of vital relevance in sustaining the catalytic cycle. This study also provides experimental evidence for migration of one of the reaction intermediates (NO_2) across the surface, which was postulated to be an important mechanistic step in oxygen inter-site transport processes involved in the direct decomposition of NO over CuZSM-5 catalysts [46].

4. Conclusions

Interaction of NO with Ni^{II}/SiO_2 catalyst provides a useful functional model for understanding the interfacial coordination chemistry of NO. The observed reactivity can be rationalized in terms of NO disproportionation reaction associated with alternations of the nickel oxidation states. The multi-step reaction involves incipient formation of mono ($\{Ni_{3c}–NO^{\bullet}\}^9/SiO_2$) and dinitrosyl ($\{Ni_{2c}–(NO)_2\}^{10}/SiO_2$) complexes, reduction of nickel to $\{Ni^{I}{}_{3c}–NO^{\delta+}\}^9/SiO_2$ via an electron transfer, oxygenation of metal ion by NO to form a nickel-oxo complex, formation of $\{Ni_{3c}–NO_2\}^9/SiO_2$ species, and spillover of the NO_2 ligand onto silica. The key intermediates appearing during the whole reaction have been isolated and identified by joint use of EPR and IR techniques complemented with DFT calculations.

Acknowledgments

Financial support by the Committee for Scientific Research of Poland, KBN, grant number 3 T09A 147 26 is acknowledged. The calculations were carried out with the computer facilities of CYFRONET–AGH, the Academic Computing Center, under grant number KBN/SGI2800/UJ/018/2002. Z.S. is grateful to the Université Pierre et Marie Curie, Paris VI, for an invited Professorship.

References

[1] R. Eisenberg, D.E. Hendriksen, Adv. Catal. 28 (1979) 79.
[2] M. Mihaylov, K. Hadjiivanov, Langmuir 18 (2002) 4376.
[3] P. Pietrzyk, E. Kukulska-Zajac, D. Lorens, Z. Sojka, J. Datka, Stud. Surf. Sci. Catal. 154 (2004) 1589.
[4] D. Gwost, K.G. Caulton, Inorg. Chem. 13 (1974) 414.
[5] R. Eisenberg, C.D. Mayer, Acc. Chem. Res. 8 (1975) 26.
[6] D. Costa, G.M. Martra, M. Che, L. Manceron, M. Kermarec, J. Am. Chem. Soc. 124 (2002) 7210.
[7] J.Y. Carriat, M. Che, M. Kermarec, M. Verdaguer, A. Michalowicz, J. Am. Chem. Soc. 120 (1998) 2059.
[8] P.H. Kasai, R.J. Bishop, D. McLeod, J. Phys. Chem. 82 (1978) 297.
[9] P.H. Kasai, R.M. Gaura, J. Phys. Chem. 86 (1982) 4257.
[10] H. Choo, S.B. Hong, L. Kevan, J. Phys. Chem. B 105 (2001) 1995.
[11] M.A. Djieugoue, A.M. Parkash, L. Kevan, J. Phys. Chem. B 103 (1999) 804.
[12] H. Choo, A.M. Parkash, S.K. Park, L. Kevan, J. Phys. Chem. B 103 (1999) 6193.
[13] T. Spalek, P. Pietrzyk, Z. Sojka, J. Chem. Inf. Model. 45 (2005) 18.
[14] DMol, InsightII, Release 2000.1; Accelrys Inc., San Diego, CA, 2000.
[15] S.H. Vosko, L. Wilk, M. Nusair, Can. J. Phys. 59 (1990) 1200.
[16] A.D. Becke, J. Chem. Phys. 88 (1988) 2547.
[17] J.P. Perdew, Y. Wang, Phys. Rev. B 45 (1992) 13244.
[18] M.J. Frisch, G.W. Trucks, H.B. Schlegel, G.E. Scuseria, M.A. Robb, J.R. Cheeseman, V.G. Zakrzewski, J.A. Montgomery, R.E. Stratmann, J.C. Burant, S. Dapprich, J.M. Millam, A.D. Daniels, K.N. Kudin, M.C. Strain, O. Farkas, J. Tomasi, V. Barone, M. Cossi, R. Cammi, B. Mennuci, C. Pomelli, C. Adamo, S. Clifford, J. Ochterski, G.A. Petersson, P.Y. Ayala, Q. Cui, K. Morokuma, D.K. Malick, A.D. Rabuck, K. Raghavachari, J.B. Foresman, J. Ciosłowski, J.V. Ortiz, B.B. Stefanov, G. Liu, A. Liashenko, P. Piskorz, I. Komaromi, R. Gomperts, R.L. Martin, D.J. Fox, T. Keith, M.A. Al-Laham, C.Y. Peng, A. Nanayakkara, C. Gonzalez, M. Challacombe, P.M.W. Gill, B.G. Johnson, W. Chen, M.W. Wong, J.L. Andres, M. Head-Gordon, E.S. Replogle, J.A. Pople, Gaussian98, Revision A.6., Gaussian, Inc., Pittsburgh, PA, 1998.
[19] P. Pietrzyk, W. Piskorz, Z. Sojka, E. Broclawik, J. Phys. Chem. B 107 (2003) 6105.
[20] G. te Velde, F.M. Bickelhaupt, S.J.A. van Gisbergen, C. Fonseca Guerra, E.J. Baerends, J.G. Snijders, T. Ziegler, J. Comput. Chem. 22 (2001) 931.
[21] ADF2002.03, SCM, Theoretical Chemistry, Vrije Universiteit, Amsterdam, The Netherlands (http://www.scm.com).
[22] E. van Lenthe, P.E.S. Wormer, A. van der Avoird, J. Chem. Phys. 107 (1997) 2488.
[23] G. Schreckenbach, T. Ziegler, J. Phys. Chem. A 101 (1997) 3388.
[24] J.M. Garot, C. Lepetit, M. Che, P. Chaquin, J. Phys. Chem. A 105 (2001) 9445.
[25] D. Biglino, H. Li, R. Erickson, A. Lund, H. Yahiro, M. Shiotani, Phys. Chem. Chem. Phys. 1 (1999) 2887, and references therein.
[26] D. Astruc, Electron Transfer and Radical Processes in Transition-Metal Chemistry, Wiley, New York, 1995, p. 235.
[27] T. Rudolf, A. Pöppl, W. Brunner, D. Michel, Mag. Res. Chem. 37 (1999) S93.
[28] P.W. Atkins, M.C.R. Symons, The Structure of Inorganic Radicals, Elsevier Publishing Company, Amsterdam, 1967.
[29] K. Hadjiivanov, Catal. Rev. Sci. Eng. 42 (2000) 71.
[30] P.H. Kasai, R.J. Bishop, J. Am. Chem. Soc. 94 (1972) 5560.
[31] L. Bonneviot, D. Olivier, M. Che, J. Mol. Catal. 21 (1983) 415.
[32] E. Grabowski, J.C. Vedrine, Chem. Phys. Lett. 48 (1977) 550.
[33] P. Hennebert, J.F. Hemidy, D. Cornet, J. Chem. Soc., Faraday Trans. 76 (1980) 952.
[34] S.K. Hoffman, J. Goslar, J. Solid State Chem. 44 (1982) 343.
[35] W.R. Scheidt, M.K. Ellison, Acc. Chem. Res. 32 (1999) 350.
[36] Z. Sojka, M. Che, J. Phys. Chem. 100 (1996) 14776.
[37] J.H. Lunsford, J. Colloid Interf. Sci. 26 (1968) 355.
[38] M. Zomack, K. Baberschke, Phys. Rev. B 36 (1987) 5756.
[39] R.N. Schwartz, M.D. Clark, W. Chamulitrat, L. Kevan, J. Appl. Phys. 59 (1986) 3231.
[40] Z. Sojka, Catal. Rev. Sci. Eng. 37 (1995) 461.
[41] M. Che, Z. Sojka, Topics Catal. 15 (2001) 211.
[42] F. Bottomley, Acc. Chem. Res. 11 (1978) 158.
[43] G.B. Richter-Addo, P. Legzdins, Metal Nitrosyls, Oxford University Press, New York, 1992.
[44] E. Giamello, D. Murphy, G. Magnacca, C. Morterra, Y. Shioya, T. Nomura, M. Anpo, J. Catal. 136 (1992) 510.
[45] P. Pietrzyk, Z. Sojka, Ann. Pol. Chem. Soc. 3 (2004) 503.
[46] B. Moden, P. Da Costa, B. Fonfe, D.K. Lee, E. Iglesia, J. Catal. 209 (2002) 75.